Presented at the Physics Summer School Meeting, Jindabyne, Australia, February 7 - 11, 1977

LBL-6505
c. 1

VERY HIGH-SPIN STATES IN NUCLEI

Richard M. Diamond

April 18, 1977

Prepared for the U. S. Energy Research and Development Administration under Contract W-7405-ENG-48

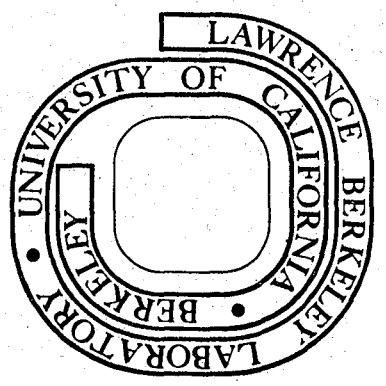

LBL-6505
c. 1

VERY HIGH-SPIN STATES IN NUCLEI*

Richard M. Diamond

Lawrence Berkeley Laboratory,
Berkeley, California, 94720,

and

Department of Nuclear Physics,
The Australian National University,
Canberra, A.C.T. 2600.

Abstract

The continuum γ-ray spectrum following neutron emission in a (HI,xn) reaction consists of a high-energy tail, the statistical cascade, and a lower-energy bump, the yrast cascade, which contains most of the intensity and consists mostly of stretched E2 transitions. Thus, a good approximation to the average angular momentum carried by the γ-rays is $2\bar{N}_{\gamma}$. Under favourable conditions, effective moments of inertia can be deduced for states up to the top of the γ-ray cascade. The maximum angular momentum in the cascades is probably limited by α-emission for nuclei with A < 150 and by fission for those with A > 150.

* Work performed under the U.S. Energy Research and Development Administration.

Today it is possible to obtain information on nuclei at very high spins, and so see whether there are differences in behaviour from that at low spins. When 100 units of angular momenta are added to a nucleus, we enter a new nuclear regime in which the rotational energy approaches the order of magnitude of the Coulomb and surface energies, and is much larger than pairing and shell effects. As a result, effects on the nuclear shape, on the moments of inertia, even on the modes of decay, might be expected, and there will be an interplay between the single-particle and collective motions to most efficiently carry the angular momentum.

The use of heavy ions has made possible the investigation of high-spin states, and there have been three principal classes of studies:

1) Heavy-Ion Coulomb excitation
2) (Heavy-ion,xnγ) reactions to study the discrete states up to spin 24-28$\hbar$
3) (Heavy-ion,xnγ) reactions to study the yrast region up to spin 60$\hbar$ via continuum γ-rays.

It is the third type of study that I would like to take up, as we want to discuss the properties and behaviour of nuclei with spins $\geq$ 30$\hbar$. Let us consider what might reasonably be expected. The first figure presents a schematic view of the excitation energy vs. angular momentum diagram for an even-even nucleus of A $\approx$ 160. Drawn across the plot is the yrast[1] line, the locus of the lowest-lying states of each spin. At low energies and spins one observes mainly the ground band, and sometimes the so-called quadrupole and octupole vibrational bands, but there are not many levels until above the pairing gap. Then the number of levels increases exponentially, and they become quite dense a few MeV up in excitation. Pairing, however, weakens with increasing spin, and the gap

is expected to disappear between spin 20-30ħ. Shell effects, on the other hand, are not expected to go away with an increase in spin, although the nucleon number at which they appear will change as a function of spin. Their magnitude is indicated roughly on the figure.

Most deformed nuclei at low excitation are prolate with axial symmetry, but as the angular momentum of the nucleus increases, pairs of nucleons may decouple from the deformation axis and align their spin with the axis of collective rotation[2]. This particle motion breaks the axial symmetry, and the nucleus becomes triaxial. If more and more pairs of nucleons decouple and align with the rotation axis, as is expected, an increasing fraction of the total angular momentum will be carried by the aligned particles rather than by the collective rotation of the core. If all the particles in the unfilled shell become aligned, the nucleus may become oblate with all these particles going around the rotation axis which is now also the symmetry axis[3]. At a still higher spin, the nucleus may start to stretch dramatically and become triaxial again before fissioning[4]. The initial fission barrier for zero spin in this case is $\sim$ 40 MeV, but decreases with spin, as shown in the figure, and becomes zero about I = 90.

That is what we might expect. I would like to use the same sort of diagram to show you what we actually know in Figure 2. Below $\sim$ 3 MeV and I $\sim$ 20, we know a lot. We have seen the ground-band levels and have measured many of their properties. We have observed β- and γ-bands and octupole bands, and have seen the curious results of band crossings known as backbending[5]. But above that region we know increasingly little. We do know that the time from the formation of the compound system to the observation of discrete transitions in the ground band is fast, some few picoseconds, in the dozen or so measured cases[6-8]. And there is a cut-off at high spin which has been determined from the sum of the evaporation residue cross sections, assuming a sharp cut-off model for the collision[9-12].

So the problem is to learn more about the high-spin states above I = 30, especially those along the yrast region where the nucleus is thermally cool and does not have a high density of states. One might consider irradiating a target with a heavy-ion beam to bring in 50-100ħ and then study the de-exciting γ-rays to obtain the energy-level spacings, the branching ratios, multipolarities, the moments of inertia, etc., as already done for spins $\leq$ 20ħ. In fact, the problem is not so simple. Bombardment of an A = 80-150 target with Ar or Kr can involve up to 100ħ in the collision, but not all collisions yield compound nuclei. The distant collisions, those with the largest impact parameters, are the high angular momentum collisions, but they mostly go into direct reactions, into quasi-elastic transfer reactions, deep-inelastic scattering, and prompt fission. However, summing the experimental cross sections for evaporation residues,

$$\sum_i \sigma_i = \pi \lambda\!\!\!^{-2} \ell_{e.r.}(\ell_{e.r.}+1) \qquad (1)$$

indicates that ℓ-waves up to ℓ = 60 are involved in the xn reaction products. That is, there are states with spins that high in the initial compound nucleus that lead to the observed evaporation residue products.

Figure 3 shows the low-energy portion of two γ-ray spectra of the de-excitation of ^{166}Yb taken with Ge counters. The discrete lines of the ground-band transitions fade out about spin 14^+, but the "background" goes on for several MeV, though decreasing in intensity. But this is not a background in the usual sense; for example, it is not the room background, which has already been subtracted. A gate set at 1 or 2 MeV brings back the same spectrum in another Ge counter that is in coincidence with the first one. Both the discrete lines and the continuous "background" appear. The latter is a continuum of γ-ray lines that lie above the discrete ground-band transitions and cascade into them. The individual transitions cannot be seen, we think, because there are too many of them sharing the intensity

to be resolved by our Ge counters. But this continuum of γ-rays represents more intensity than is present in the discrete transitions observed, and is our only direct experimental contact or connection with the initial high-spin states in these nuclei.

So let us look just once more at the plot of excitation energy vs. I in Figure 4 and consider[13] the course of an (^{40}Ar,4nγ) reaction after the initial production of compound nuclei with A ∿ 160. With an ^{40}Ar bombarding energy of 170-175 MeV, these initial nuclei will have an excitation energy of ∿ 70 MeV and a distribution of angular momenta from 0 up to a value of about 60ħ. The first step in the de-excitation process is the emission of neutrons; each one takes away its binding energy plus, on the average, 2T of kinetic energy, where T is the nuclear temperature, a total of 10-15 MeV. The distribution in kinetic energies fuzzes out the value of the excitation energy of the residual nuclei, the more so the larger the number of neutrons emitted, but since the neutrons carry off little angular momentum, they leave the spin distribution relatively unchanged. When the excitation energy is just less than a neutron binding energy above the yrast line, γ-ray emission takes over[14]. This limit after the emission of four neutrons is shown by the heavy line in Figure 4. Several MeV above the yrast line there is still a high density of levels, so γ-rays from this region are probably dipole transitions statistically distributed in energy. They, too, carry off energy but little angular momentum, and so they, also, change the spin distribution little. But approaching the yrast line the level density becomes small, and the γ-rays must carry off angular momentum as well as energy and so move parallel to the yrast line. Since we know that the entire γ-ray cascade takes only picoseconds, the individual transitions have lifetimes of tenths or even hundredths of a picosecond, and most likely are stretched E2 transitions moving down collective bands. There must be a dozen or more such bands dividing up the intensity, as we cannot

resolve the individual lines[13]. And for the same reason, the intensity must stay distributed in the different bands and not gather in the lowest band, at least not until about spin 20 where discrete lines usually begin to be observed. One other feature may be expected, namely, that more neutrons are emitted from compound nuclei with low spin than from those with high spin. This arises simply because there is more thermal excitation energy available (the difference between the initial excitation energy and the yrast line) at low spin than at high spin where tens of MeV are tied up in the rotation of the nucleus as a whole. As a result, there will be some fractionation of the final products depending upon the initial angular momentum. This is why the heavy line in Figure 4 indicating the region leading to a 4n product does not cover the entire angular momentum distribution available to the initial compound nuclei. However, the upper and lower cut-offs are not sharp as shown in the figure. But this feature is of importance to our studies, for we will observe the highest spin states in the γ-ray cascades by picking out the reaction channel with the fewest neutrons.

Our basic experimental set-up to study continuum γ-ray spectral shapes[15c] is shown in Figure 5. There is a Ge counter placed at -125° to the beam direction and 5 cm from the target, a $\sim$ 1 mg/cm^2 foil on a 25 μm Pb backing. This counter is in coincidence, pairwise, with three 7.5 × 7.5 cm NaI(Tℓ) detectors at 0°, 45° and 90° to the beam and 60 cm back from the target. Setting windows on known discrete lines in the Ge counter brings back the γ -ray spectrum associated with a particular reaction channel in the NaI detectors, and the Ge counter also provides a start signal in order to distinguish neutron and γ-ray events at the NaI counters by time of flight. Other types of start signals and experimental arrangements have been used by other groups[15-24], and, for example, we and others have used a particle telescope when studying multiplicities in deep-inelastic scattering[25].

Figure 6 shows a Ge spectrum for the de-excitation cascades resulting from the irradiation of ^{126}Te with 181 MeV ^{40}Ar. When gates are placed on the discrete lines corresponding to the 4n reaction channel, thereby picking out the cascades of ^{162}Yb alone, the raw coincidence NaI spectrum shown in Figure 7 with hollow squares is obtained[15c]. It is obvious even from this spectrum that a gross structure is present, namely a high-energy exponential tail and a low-energy "bump". But we must unfold this pulse-height spectrum with the detector response function in order to get back the original γ-ray distribution. This is done by means of a computer program[26] whose parameters have been determined by running standard sources in the same detector arrangement as used in the experiment. If we also divide the spectrum by the efficiency of the NaI detector and by the number of Ge counter singles gates, and make a small correction for Doppler shift, we get the absolute number of transitions per energy interval (40 keV in our case). This is plotted as the filled circles with the left-hand scale as ordinate. The integral of this curve over all transition energies is the average number of γ-rays per event. It is the average γ-ray multiplicity for that (4n) reaction channel, and will be symbolized by $\overline{N}_\gamma$. The unfolded spectrum shows the two components more clearly perhaps, and the ratio of intensities for the 0°/90° angular correlation given at the top of Figure 7 suggests that the bump region, containing most of the γ-rays, is made up of stretched E2 transitions, while the higher-energy exponential tail is probably mixed dipole-electric quadrupole.

If the bump transitions are indeed all stretched E2's as indicated, then we can approximately determine the average angular momentum, $\overline{\ell}$, carried by the cascades for a particular reaction channel by $2(\overline{N}_\gamma - \delta)$, where δ is the number of statistical γ-rays effectively carrying off no angular momentum. (Empirically this number seems to be 2-4.) That is,

$$\overline{\ell} = 2(\overline{N}_\gamma - \delta) \qquad (2)$$

This is an important and very useful relation, if true. Is there any independent evidence bearing on this point?

There is. If we assume a sharp cut-off model of the nucleus, we can obtain an estimate of the largest value of ℓ leading to a particular xn reaction product from the sum of the cross sections leading to that product or to any higher xn product. By assuming an angular momentum distribution, e.g. the classical triangular one, we can calculate from this upper value of ℓ the average value of ℓ involved in that reaction channel, $\overline{\ell}(\sigma)$, and then compare it with the value deduced from the multiplicity. Such a comparison[27] is shown in Figure 8 where values of $\overline{N}_\gamma$ are plotted vs. $\overline{\ell}(\sigma)$ for two dozen reaction channels involving some de-excitation cascades from ^{170,168}Yb compound nuclei, but mainly from ^{166}Yb. The compound systems were produced with ^{16}O, ^{40}Ar and ^{86}Kr beams (from the Berkeley 88" cyclotron and Super-HILAC), and there is no trend or differentiation whatsoever with the nature of the projectile. But there clearly is a strong correlation between $\overline{N}_\gamma$ and $\overline{\ell}(\sigma)$, although the slope is not 1/2 as required by Eq. 2. The line arbitrarily drawn through the points has a slope of 0.43, which corresponds to 2.3$\hbar$ carried per γ-ray, rather than 2.0 for stretched E2 transitions. We know from the measured cascade decay times that no octupole transitions can be involved (too long-lived). But there are at least two reasons for observing values greater than 2. Firstly, the value of $\overline{\ell}(\sigma)$ obtained from the cross sections is the average angular momentum before neutron emission, and so must be decreased by the angular momentum carried away by the neutrons before comparing with the average spin value deduced from the γ-ray multiplicity. In addition, when high spins are involved, the statistical γ-rays may carry off some angular momentum. Secondly, $\overline{\ell}(\sigma)$ has been calculated assuming that each reaction channel takes a certain

exclusive range of angular momenta. Since the channels are certainly not that distinctly fractionated in spin, there must be some overlap in their range of spin values. If so, the average value for a reaction channel in a high-spin range will be lower than has been calculated, and that for a channel in a low-spin range will be higher. This effect certainly helps account for the deviation from slope 1/2. So Eq. 2 appears justified, and the intercept on the y-axis suggests that there are ~ 4 statistical γ-rays that carry away no angular momentum, at least at low spin. But the main point to be drawn from Figure 8 is that $\bar{\ell} \approx 2\bar{N}_\gamma$ for all but low multiplicities.

Looking now at the bottom curves in Figure 7, the unfolded spectrum (from the upper part) has been redrawn as a solid curve and can be compared with the unfolded spectrum for the same 4n reaction channel, but at a lower (157 MeV) average ^{40}Ar bombarding energy and from the ^{150}Sm(^{16}O,4n) reaction with 87 MeV ^{16}O. These last two reactions have very similar (estimated) angular momentum inputs, and show essentially identical spectra, though quite different from that with 181 MeV ^{40}Ar. The main difference at the higher energy appears to be displacement of the yrast bump horizontally to higher energy, corresponding to about six more γ-rays in the cascade and so to 12 units more angular momentum in the initial nuclei leading to this reaction channel.

Figure 9 gives the unfolded spectra from additional reaction channels[27], namely the (^{16}O,5n) with 87 MeV ^{16}O and the (^{40}Ar,3n) with 157 and (^{40}Ar,5n) with 181 MeV ^{40}Ar. In each case when one compares the spectra at a particular bombarding energy, each fewer neutron emitted means an increase in the upper energy of the bump and an increase in the area under the bump corresponding to ~ 6 γ-rays ($\sim 12\hbar$ more angular momentum in the initial compound nuclei). This is a clear indication of the expected fractionation of the reaction products according to the angular momentum distribution of the original compound nuclei. That is, those nuclei with the largest

amount of angular momentum emit fewer neutrons and more γ-rays than those with smaller amounts of angular momentum. More importantly, increasing multiplicity, hence angular momentum, seems to go with a higher yrast bump edge in these examples. If we associate the edge energy with the transitions from states of highest spin, as is true for a rotor, then we can determine the effective moments of inertia, J, at these high spins[15c] from

$$E_\gamma = \frac{\hbar^2}{2J}(4I-2), \qquad (3)$$

the expression for the transition energies of a rotor. The same expression can also be used at transition energies below the edge if they are low enough so that there is no appreciable direct population into the reaction channel. Such determinations of the effective moments of inertia are shown in Figure 10 where $2J/h$ is plotted vs. $\hbar^2\omega^2$ (essentially $(E_\gamma/2)^2$) in a conventional backbending plot for ^{162}Yb. The discrete transitions of the ground band are shown as filled circles. We were not able to find still higher transitions, which, presumably, might go through a backbend, and so have also plotted the values for the isotone ^{160}Er (open circles), which is known through a backbend to spin 22^+. The values of $2J/\hbar^2$ determined from the bump edges are shown as the three solid symbols at high $\hbar\omega$, and the use of Eq. 3 at lower energies below the region of direct population gives the large solid circles. Values obtained by a differential method of calculating moments of inertia, but also only for the region of transition energies below direct population after neutron emission, are shown by the filled diamonds. All these values are in reasonable agreement with each other, and since they depend on different assumptions, we believe they are correct within their indicated errors. They are near the value calculated for a rigid diffuse sphere with $A = 162$, shown as a dashed line in the figure, and fall only slightly

below the liquid-drop values, which would be equal to the rigid sphere at low spin (or $\hbar\omega$) and $\sim$ 10% larger at the highest point ($I \sim 60$).

All of the examples so far have been of Yb nuclei; let us look at a somewhat lower region of the periodic table. Consider the case $^{40}Ar + {}^{82}Se \rightarrow {}^{122}Te^{*}$. Figure 11 shows the raw data of the γ-ray continuum spectrum for the 4n reaction channel as seen by the NaI counter, and above it is drawn the unfolded spectrum (scale on the left)[28]. The same sort of gross structure is observed; there is the high-energy exponential tail of the statistical γ-rays, and the lower energy bump containing most of the intensity and coming, presumably, from the many cascades along the yrast region. In agreement with this, the anisotropy of the angular correlation, the ratio of intensities at 0° to that at 90° shown at the top of the figure, again indicates stretched E2 transitions for the bump region. The unfolded spectrum also shows some finer structure. There are two sharp peaks at about 600 and 800 keV, a valley just above 1 MeV, possibly a small peak at $\sim$ 1.4 MeV, and a broad peak just below 2 MeV. The low-energy peaks are easily understood. The 2^{+}, 4^{+} and 6^{+} states in ^{118}Te de-excite by means of 605, 601, 615 keV transitions, and these create the first peak, which, in fact, integrates to three transitions. We have studied the energy-level scheme of ^{118}Te, and the next four higher states give four lines which make up the 800 keV peak. The higher energy features are not so easy to explain, but the existence of a valley followed by a broad peak at higher energy indicates a change in nuclear structure, a definite increase in γ-ray transition density. It might even correspond to a giant backbend at high spin; we do not know at this time.

An interesting point is that Ragnarsson and Soroka, two young theoreticians at Berkeley, have calculated the transition energy spectrum along the yrast line for ^{118}Te by adding shell corrections to the liquid-drop values[29]. They knew of our interest in this nucleus, but did their

calculations quite independently of our experiments. Their result is shown in Figure 12 where the transition energies are plotted vs. spin. The curve is the liquid-drop result, the unfilled circles are the known levels to 14^+ in ^{118}Te, and the filled circles are their shell-corrected energies, starting with the $20 \rightarrow 18$ transition (as they did not include pairing in their calculations). These points correspond in the unfolded spectrum to a valley around 1 MeV, a peak at 1.5 MeV, and a larger peak just above 2 MeV. I am not trying to say there is a one-to-one correspondence between calculation and experiment, as I do not believe either one is accurate enough yet to draw such conclusions. I am only pointing out that both experiment and theory suggest that there should be finer structure in the unfolded spectra, and that, hopefully, in the future we may achieve an accuracy for both which will permit a real comparison.

Figure 13 shows unfolded spectra[28] for the γ-ray cascades from ^{118}Te made by 51 and 75 MeV (^{12}C,4n) on ^{110}Pd and 161, 171 and 181 MeV (^{40}Ar,4n) on ^{82}Se. With irradiation by 51 MeV ^{12}C one is less than 10 MeV above the Coulomb barrier and so less than 22 units of angular momentum are brought to the compound nucleus, even before neutron emission. One sees the ground-band transitions up through the $14 \rightarrow 12$, but there is little of the yrast bump, since few decays involve much higher spin states. Even with the 75 MeV ^{12}C run, there is little to the yrast bump. But with the use of ^{40}Ar projectiles, considerably larger amounts of angular momentum are brought to the nuclei and large yrast bumps result. An interesting feature in Figure 13 is that with an increase in bombarding energy, and hence increase in angular momentum brought to the nucleus, there appears to be little change in the high-energy edge of the yrast bump. This is in contrast to the situation in the Yb nuclei shown in Figures 7 and 9. The occurrence of a relatively fixed edge to the bump in ^{118}Te might come about because of a backbend in the transition energies at that point, but we believe that it

is more likely due to a limitation caused by α-emission from near the yrast line at sufficiently high spin values (determined by the steepness of the line, as described below). There will certainly be limitations on how much angular momentum can be accommodated by a nucleus, and this is the final topic I would like to discuss.

I have mentioned earlier that, at least with the heavier targets, fission (or, with heavy projectiles, quasi-fission) is the most likely result from high angular momentum collisions. Figure 14, taken from the paper by Cohen, Plasil and Swiatecki[30], shows, as a function of mass number, the angular momentum at which the fission barrier of a liquid-drop nucleus falls to zero. Also shown is the curve for a barrier of ∿ 8 MeV, which seems to correspond to the cut-off to the evaporation residue cross sections found experimentally. On the average, nuclei with more angular momentum than this fission before getting to the γ-ray cascade, thus creating limits to both the transition energies, $E_\gamma(\max)$, and the spins, $I(\max)$.

But for lighter nuclei, A < 150, we believe that α-emission is the limitation, and by that we mean α-emission from the yrast line and the region just above the line, in contrast to the α-emission that may take place at high excitation[31]. For sufficiently steep yrast lines (high I and low A), the decrease in energy for the change of a few units in I is large enough to equal the binding energy plus Coulomb and centrifugal barriers for emission of an α-particle. For any given nucleus whose yrast line is assumed (usually taken at high spins to be that of a rigid rotor), values of $I(\max)$, $E_\gamma(\max)$, and ΔI, the angular momentum carried off by the particle, can be calculated for the point where the probabilities for γ-decay and particle decay are equal. For the γ-rays we used an average enhanced reduced transition probability, $B(E2)\downarrow = 1.6\left(\frac{Z}{66}\right)^{3/2}\left(\frac{A}{162}\right)^{4/3} e^2b^2$, and for the particles[32], $\Gamma(P) = T_\ell(P)\ D/2\pi$, where $T_\ell(P)$, the transmission coefficients, were taken from optical model codes and D, the level spacing, was assumed

to have the value 30 keV or 3 keV at I = 40 for A = 104. These numbers provide a plausible, but not necessarily correct range of values; however, calculations with them do seem to straddle the experimental results. To allow for the variation of D with A and I, we used the triaxial rotor model of Bohr and Mottelson for the yrast region[33], yielding $D \propto IA^{-5/3}$, if the shape of the nucleus were independent of A and I. (Not true, but not serious, in general.) There are lots of ifs and assumptions in the analysis, but the results must be grossly right, though probably wrong in detail. The analysis shows that the limiting angular momenta for proton and neutron emission along the yrast region in these moderately neutron-deficient nuclei are considerably higher than those for α-emission. Hence, the latter provides the limit shown in Figure 15, where E_γ(max) and I(max) are plotted vs. Z. Below A $\sim$ 150 or Z $\sim$ 60, α-emission along the yrast region provides the limit on the angular momentum brought into compound-nuclear residues[34]. It can be seen in the figure that E_γ(max) in this region changes relatively slowly, increasing from $\sim$ 2.5 MeV at Z = 60, to $\sim$ 3.5 MeV at Z = 32, and that I(max) becomes quite low at low Z. The actual experimental limits, however, will not be as smooth as the curves drawn because of shell effects; the latter have been neglected in the analysis.

We can compare these predictions with a final set of experiments[34]. Targets of ^{12}C, ^{27}Al, KCl, Ti, Fe, ^{68}Zn, ^{82}Se, $^{126,130}Te$, 0.5 - 1.2 mg/cm^2 thick deposited on 0.025 mm Pb, were bombarded with ^{40}Ar beams of a number of energies between 119 and 185 MeV. A "multiplicity filter" was used, consisting of six 7.5 × 7.5 cm NaI detectors placed symmetrically around the beam pipe and upstream from the target. These counters were in pairwise coincidence with a seventh 7.5 × 7.5 cm NaI detector placed at 45° to the beam direction and 60 cm from the target, and were electronically coded to indicate how many fired simultaneously with each event in the special NaI

detector. That is, the number of counters in coincidence with the special counter, the coincidence "fold" (a number from 1 to 6) was recorded for each event. From the distribution of folds, the multiplicity could be determined as a function of E_γ in the special counter. Typical results are shown in Figures 16 and 17. In Figure 16 are given plots of $\bar{N}_\gamma$ vs. E_γ for the reaction products resulting from ^{82}Se irradiated with ^{40}Ar at the various initial energies listed. The lowest bombarding energy, 119 MeV, is just at the barrier, but the characteristic feature of the curves for the higher energies is the growth of a multiplicity peak around E_γ = 2 MeV. Since the highest γ-ray energy in a rotational cascade, $E_\gamma(max)$, will correspond to the highest angular momentum, and hence highest multiplicity, this peak identifies directly $E_\gamma(max)$, for the nucleus and bombarding energy considered, as being at its leading edge. This edge shows a slow increase in energy to just above 2 MeV, which value was indicated in Figure 15. The peak multiplicity corresponds to the highest multiplicity for any reaction channel, but somewhat lowered by dilution with statistical γ-rays. On the other hand, for E_γ greater than 3-4 MeV, we have only statistical γ-rays which occur at all angular momenta, so they represent the average γ-ray multiplicity over all the reaction channels. This average rises with bombarding energy up to 161 MeV, but at 185 MeV it falls slightly (as does the multiplicity peak). The reduction is due to the onset of new reactions of lower average γ-ray multiplicity; for this nucleus it is most likely α-emission (carrying off large amounts of spin), and, indeed, we do observe large numbers of α-particles.

For compound nuclei of lower Z, similar behaviour occurs; the plots of $\bar{N}_\gamma$ vs. E_γ shown in Figure 17 are for 161 MeV ^{40}Ar, except for ^{130}Te (185 MeV) and ^{12}C (131 MeV). The multiplicity peak seems to disappear for compound systems below $Z \sim 35$. It is from such plots that the experimental values of $E_\gamma(max)$ and I(max) shown in Figure 15 are obtained, and

from the essential agreement between the points and the calculated curves, we conclude that the picture of angular momentum limitation by α-emission below A ∿ 150 and by fission above A ∿ 150 is generally valid. The highest spins in compound-nuclear residues should be obtained around A ∿ 150.

I hope I have convinced you that exciting information about high-spin states is contained in the γ-ray continuum cascades, and that we are now just beginning to develop the techniques to obtain that information. I would like to summarize my talk in the following sentences.

1. Continuum spectra have a gross structure; they usually consist of an "yrast bump" and a "statistical" tail.

2. For medium to heavy nuclei, the yrast bump contains most of the γ-rays, and they are stretched E2 transitions. An approximate value for the angular momentum carried by the γ-cascade is $2\overline{N}_\gamma$.

3. There is evidence for fractionation of the reaction products with the angular momentum of the initial compound nuclei. The difference in angular momentum per neutron emitted is ∿ 12h with the heavy-ion projectiles used.

4. Under favourable conditions, effective moments of inertia can be determined up to I(max), 50-60h for the Te and Yb nuclei studied.

5. Continuum γ-ray spectra may show finer details of nuclear structure, e.g. backbends.

6. The maximum angular momentum in yrast cascades is probably limited by fission for A > 150 and by α-emission along the yrast region for A < 150.

Acknowledgements: The work described in this talk was carried out by a number of very capable visitors and postdoctoral fellows at the Lawrence Berkeley Laboratory: Drs. P.O. Tjøm, M. Banaschik, R.S. Simon, P. Colombani, D. Soroka, J.O. Newton, I-Y. Lee, M. Aleonard, and Y. El Masri, all of whom are thanked for much hard work and many interesting discussions. The many hours of effort by the crews of the 88" cyclotron and the Super-HILAC are gratefully appreciated, as also the electronics help of Mr. M. Lee and computer programming by Mr. D. Lebeck. A special thanks goes to my partner, Frank Stephens; without his efforts much of this work would not have started, much less succeeded.

REFERENCES

1. J.R. Grover, Phys.Rev. 157, 832 (1967)

2. F.S. Stephens, Rev.Mod.Phys. 47, 43 (1975)

3. A. Bohr and B.R. Mottelson, Physica Scripta 10A, 13 (1974)

4. G. Andersson, S.E. Larson, G. Leander, P. Möller, S.G. Nilsson, I. Ragnarsson, S. Åberg, R. Bengtsson, J. Ondek, B. Nerlo-Pomorska, K. Pomorski and Z. Szymanski, Nucl.Phys. A268, 205 (1976)

5. A. Johnson, H. Ryde, J. Sztarkier, Phys.Lett. B34, 605 (1971)

6. R.M. Diamond, F.S. Stephens, W.H. Kelly and D. Ward, Phys.Rev. Lett. 22, 546 (1969);
J.O. Newton, F.S. Stephens and R.M. Diamond, Nucl.Phys. A210, 19 (1973)

7. D. Ward, H.R. Andrews, J.S. Geiger and R.L. Graham, Phys.Rev.Lett. 30, 493 (1973); N. Rud, D. Ward, H.R. Andrews, R.L. Graham and J.S. Geiger, Phys.Rev.Lett. 31, 1421 (1973)

8. W. Kutschera, D. Dehnhardt, O.C. Kistner, P. Kump, B. Povh and H.J. Sann, Phys.Rev. C5, 1658 (1972); W. Dehnhardt, S.J. Mills, M. Müller-Veggian, U. Neumann, D. Pelte, G. Poggi, B. Povh and P. Taras, Nucl.Phys. A225, 1 (1974)

9. J.B. Natowitz, Phys.Rev. C1, 623 (1970)

10. L. Kowalski, J.C. Jodogne and J.M. Miller, Phys.Rev. 169, 849 (1968); A.M. Zebelman and J.M. Miller, Phys.Rev.Lett. 30, 27 (1973).

11. H. Gauvin, Y. Lebeyec, M. Lefort and R.L. Hahn, Phys.Rev. C10, 722 (1974)

12. H.C. Britt, B.H. Erkkila, R.H. Stokes, H.H. Gutbrod, F. Plasil, R.L. Ferguson and M. Blann, Phys.Rev. C13, 1483 (1976)

13. J.O. Newton, F.S. Stephens, R.M. Diamond, W.H. Kelly and D. Ward Nucl.Phys. A141, 631 (1970)

14. J.R. Grover and J. Gilat, Phys.Rev. 157, 814 (1967)

15. a) P.O. Tjøm, F.S. Stephens, R.M. Diamond, J. de Boer and W.E. Meyerhof, Phys.Rev.Lett. 33, 593 (1974); b) M.V. Banaschik R.S. Simon, P. Colombani, D.P. Soroka, F.S. Stephens and R.M. Diamond, Phys.Rev.Lett. 34, 892 (1975); c) R.S. Simon, M.V. Banaschik, P. Colombani, D.P. Soroka, F.S. Stephens and R.M. Diamond, Phys.Rev.Lett. 36, 359 (1976)

16. E. der Mateosian, O.C. Kistner and A.W. Sunyar, Phys.Rev.Lett. 33, 596 (1974)

17. J.O. Newton, J.C. Lisle, G.D. Dracoulis, J.R. Leigh and D.C. Weisser, Phys.Rev.Lett. 34, 99 (1975)

18. G.B. Hagemann, R. Broda, B. Herskind, M. Ishihara, S. Ogaza and H. Ryde, Nucl.Phys. A245, 166 (1975)

19. M. Fenzl and O.W.B. Schult, Z. Physik 272, 207 (1975)

20. R. Albrecht, W. DÜnnweber, G. Graw, H. Ho, S.G. Steadman and J.P. Wurm, Phys.Rev. Lett. 34, 1400 (1975)

21. K.A. Geoffroy and J.B. Natowitz, Phys.Rev.Lett. 37, 1198 (1976)

22. M. Ishihara, T. Numao, T. Fukada, K. Tanaka, T. Inamura, Proc. of Sym. on Macroscopic Features of Heavy Ion Collisions, Argonne, p.617 (1976)

23. M. Berlanger, M.A. Deleplanque, C. Gerschel, F. Hanappe, M. Leblanc, J.F. Mayault, C. Ngô, D. Paya, N. Perrin, J. Péter, B. Tamain, L. Valentin, preprint 1976.

24. D.G. Sarantites, J.H. Barker, M.L. Halbert, D.C. Hensley, R.A. Dayras, E. Eichler, N.R. Johnson and S.A. Gronemeyer, Phys.Rev. C14, 2138 (1976)

25. P. Glässel, R.S. Simon, R.M. Diamond, R.C. Jared, I-Y. Lee, L.G. Moretto, J.O. Newton, R. Schmitt and F.S. Stephens, Phys.Rev. Lett. 38, 331 (1977)

26. J.F. Mollenauer, Lawrence Radiation Laboratory Report UCRL-9748 (1961)

27. R.S. Simon, M.V. Banaschik, J.O. Newton, R.M. Diamond and F.S. Stephens, to be published.

28. R.S. Simon, J.O. Newton, R.M. Diamond and F.S. Stephens, to be published.

29. I. Ragnarsson and D.P. Soroka, private communication (June, 1976)

30. S. Cohen, F. Plasil and W.J. Swiatecki, Annals of Physics 82, 557 (1974)

31. J.R. Grover and J. Gilat, Phys.Rev. 157, 823 (1967)

32. J.M. Blatt and V.F. Weisskopf, Theoretical Nuclear Physics (John Wiley and Sons, New York, 1952) p.569

33. A. Bohr and B. Mottelson, Nuclear Structure, Vol.II (W.A. Benjamin, Reading, Mass., 1975) p.191

34. J.O. Newton, I-Y. Lee, R.S. Simon, M.M. Aleonard, Y. El Masri, F.S. Stephens and R.M. Diamond, to be published.

Fig. 1. Plot of excitation energy vs. spin for a nucleus with A $\sim$ 160. Expected behaviour.

Fig. 2. Plot of excitation energy vs. spin for a nucleus with A $\sim$ 160. Known behaviour.

Fig. 3. Singles Ge de-excitation spectra of ^{166}Yb made by ^{159}Tb(^{11}B,4n) (upper curve) and ^{130}Te(^{40}Ar,4n) (lower curve).

Fig. 4. Plot of excitation energy vs. spin for a nucleus with A $\sim$ 160. Schematic illustration of γ-ray de-excitation paths following ^{40}Ar, 4n reaction.

Fig. 5. Experimental set-up used in Berkeley to study continuum γ-ray spectral shapes.

Fig. 6. Ge spectrum used for setting gates to select the continuum spectrum associated with the 4n and 5n reaction channels from the ^{40}Ar + ^{126}Te reaction.

Fig. 7. Raw (□) and unfolded (●) continuum γ-ray spectra from the ^{126}Te(^{40}Ar,4n)^{162}Yb reaction at an average beam energy of 181 MeV. The larger solid dots represent five-channel averages. At the top is shown the 0°/90° ratio for the unfolded spectra. At the bottom are shown schematic spectra for the ^{126}Te(^{40}Ar,4n)^{162}Yb reaction at 181 MeV(solid line), the same reaction at 157 MeV (longer dashed line), and the ^{150}Sm(^{16}O,4n)^{162}Yb reaction at 87 MeV (shorter dashed line).

Fig. 8. Average γ-ray multiplicity, $\bar{N}_\gamma$, plotted vs. the average angular momentum determined for a particular reaction channel from cross section measurements (see text for details).

Fig. 9. Unfolded (smoothed) continuum γ-ray spectra for the indicated reaction channels leading to Yb nuclei.

Fig. 10. Plot of $2J/\hbar^2$ vs. $(\hbar\omega)^2$ for ^{162}Yb. Filled dots are the known low-spin states, and the open dots are the known states in the backbending isotone, ^{160}Er. The large dots are values derived by the integral method for determining moments of inertia (see text) from the 181 MeV ^{40}Ar reaction. The triangle and square are for the 157 MeV ^{40}Ar and 87 MeV ^{16}O reactions. The diamonds are values from the differential method applied to the 181 MeV ^{40}Ar data. The horizontal dashed line is the moment of inertia of a rigid, diffuse sphere with A = 162.

Fig. 11. Raw (•) and unfolded (—) continuum γ-ray spectra from the ^{82}Se(^{40}Ar,4n)^{118}Te reaction at an average energy of 181 MeV. At the top is shown the 0°/90° ratio for the unfolded spectra.

Fig. 12. Transition energies for ^{118}Te calculated by Ragnarsson and Soroka from liquid-drop values (solid curve) plus shell corrections[29]. The open circles give the known ground-band transitions.

Fig. 13. Unfolded continuum γ-ray spectra for the indicated reaction channels leading to ^{118}Te.

Fig. 14. Plot of angular momenta at which liquid-drop fission barrier drops to zero vs. mass number. (ℓ_I is angular momentum at which nucleus goes triaxial.) Dashed line gives angular momentum at which fission barrier is calculated to drop to $\sim$ 8 MeV. Taken from ref. 30.

Fig. 15. Plots of E_γ(max) and I(max) vs. the atomic number. The solid lines are limits set by α-emission; the dashed lines are limits set by fission. The experimental points come from the next two figures (see text).

Fig. 16. Average γ-ray multiplicities as a function of γ-ray energy (pulse height) for spectra from ^{40}Ar + ^{82}Se at the indicated bombarding energies.

Fig. 17. Average γ-ray multiplicities as a function of γ-ray energy (pulse height) for spectra from indicated targets irradiated by 161 MeV ^{40}Ar except for ^{130}Te (185 MeV) and ^{12}C (131 MeV).

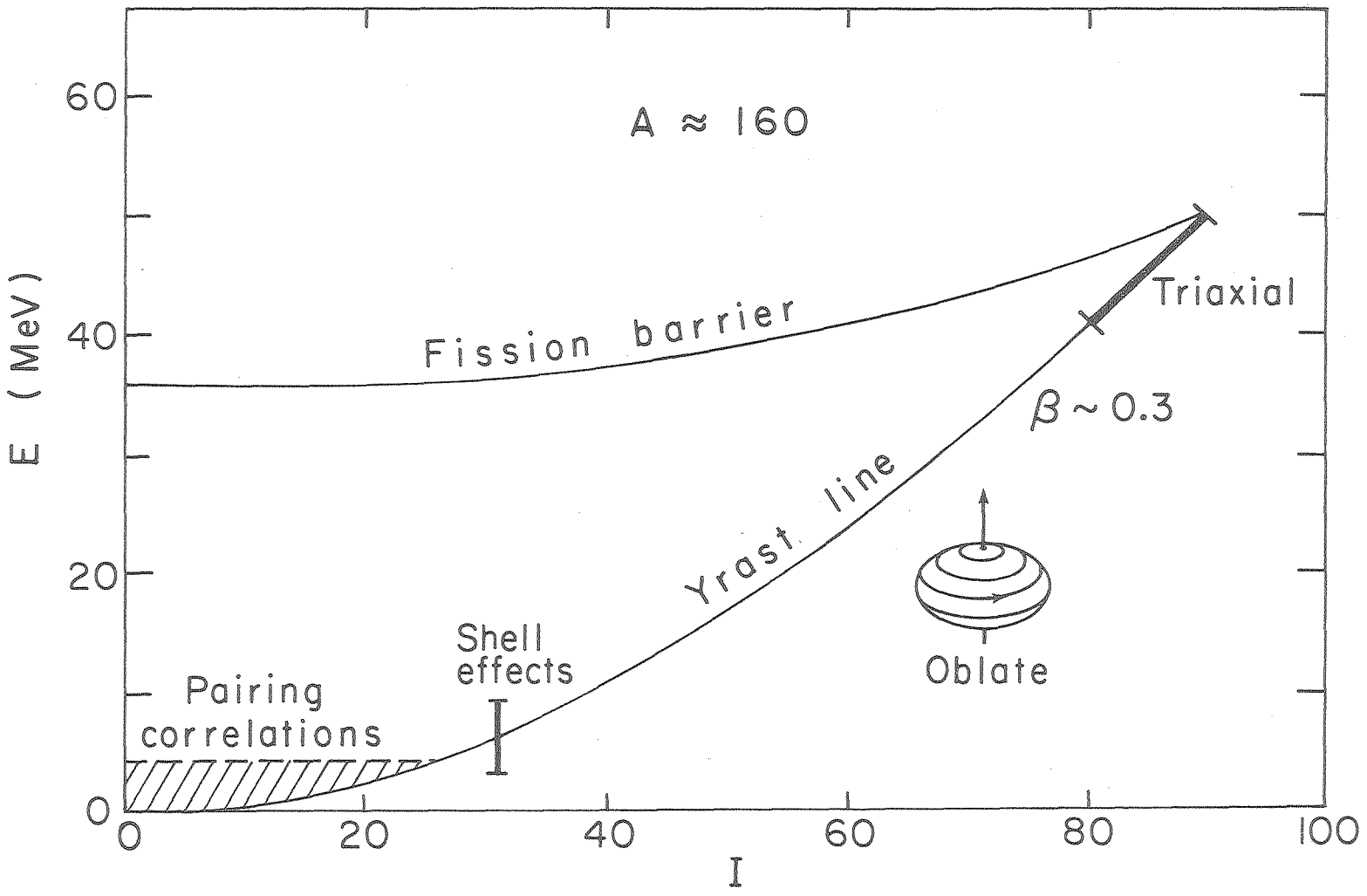

XBL7610 - 4235

Fig. 1

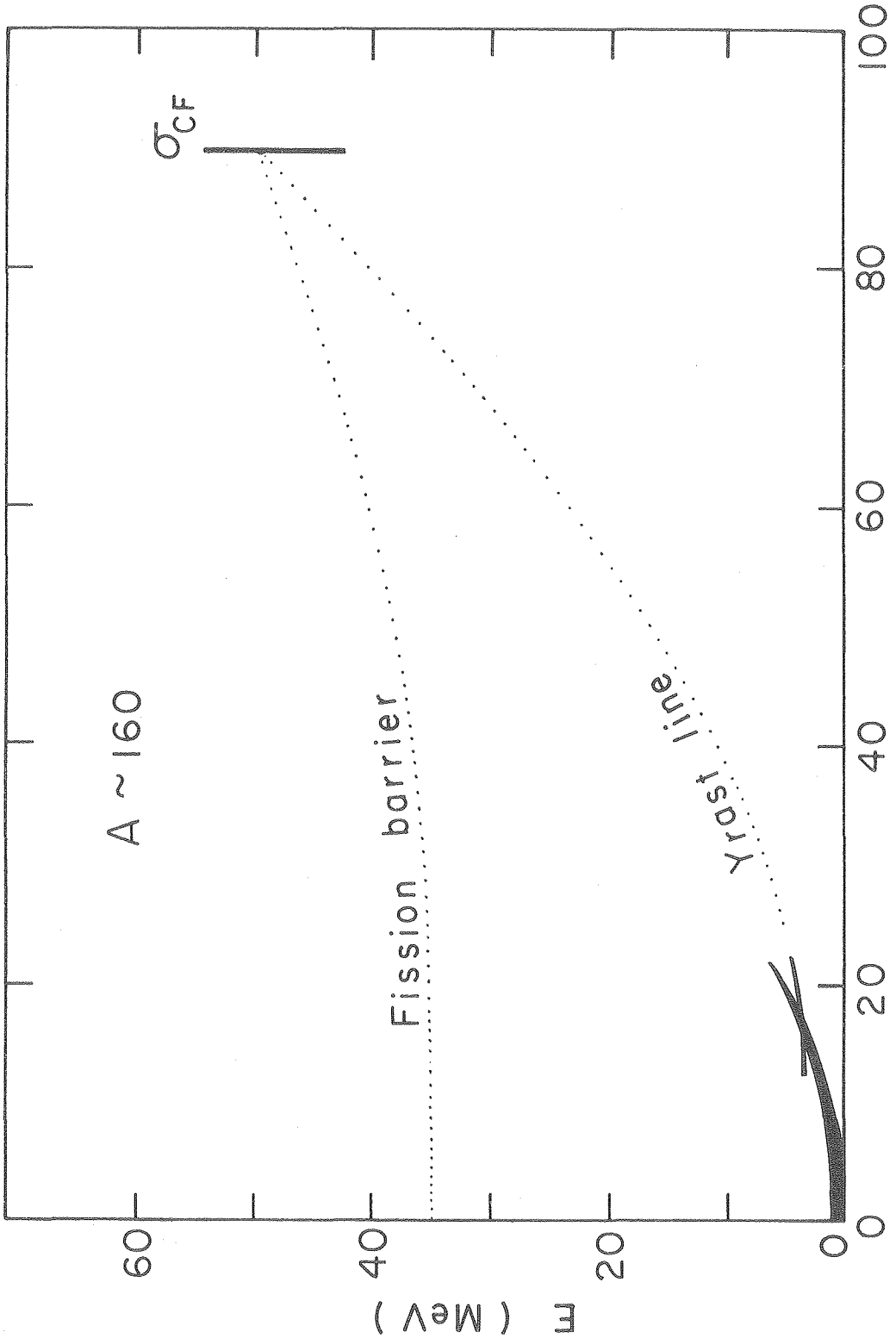

XBL7610-4233

Fig. 2

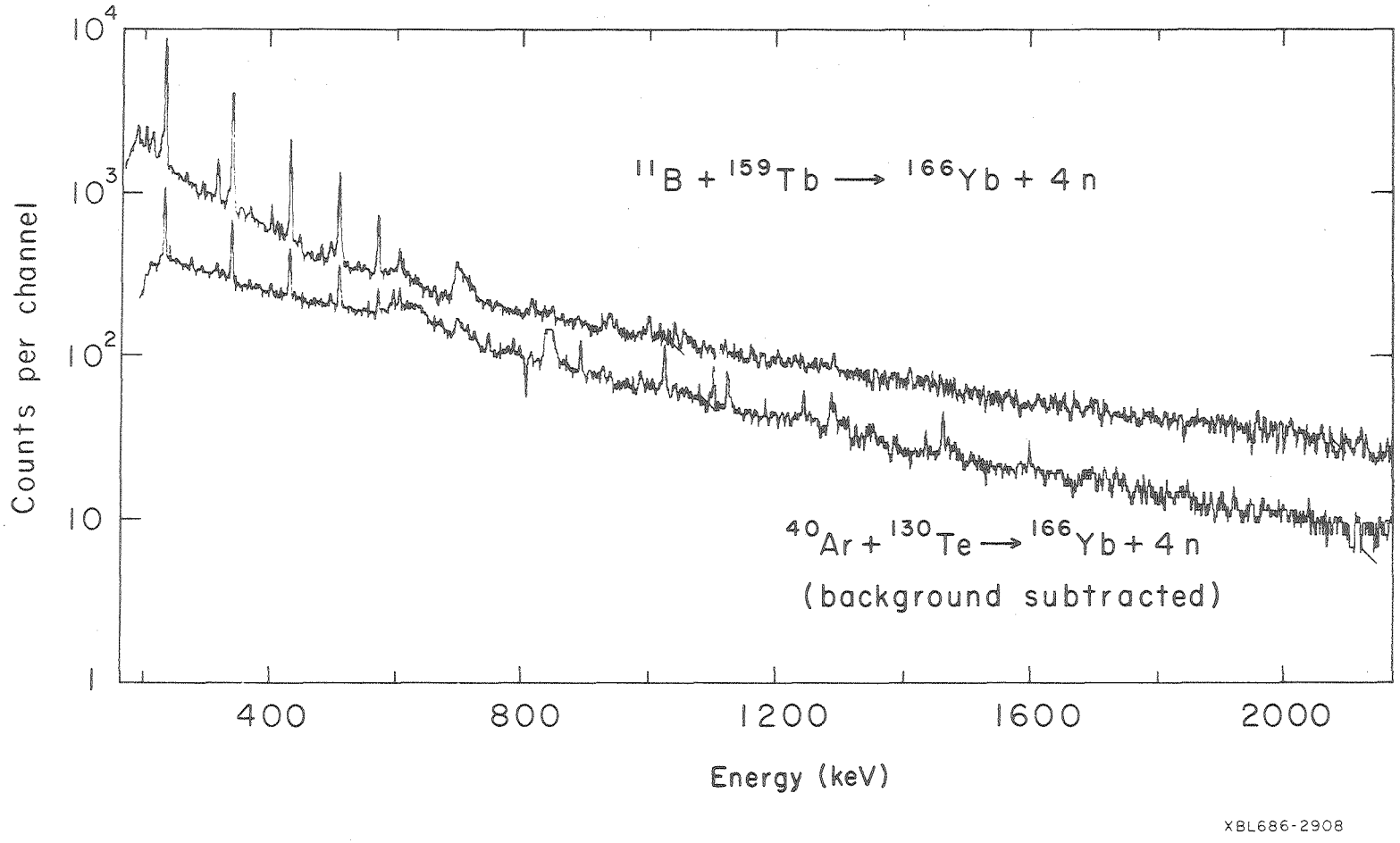
Counts per channel
10^4
10^3
10^2
10
1
400
800
1200
1600
2000
Energy (keV)
$^{11}B + ^{159}Tb \longrightarrow ^{166}Yb + 4n$
$^{40}Ar + ^{130}Te \longrightarrow ^{166}Yb + 4n$
(background subtracted)
XBL686-2908

Fig. 3

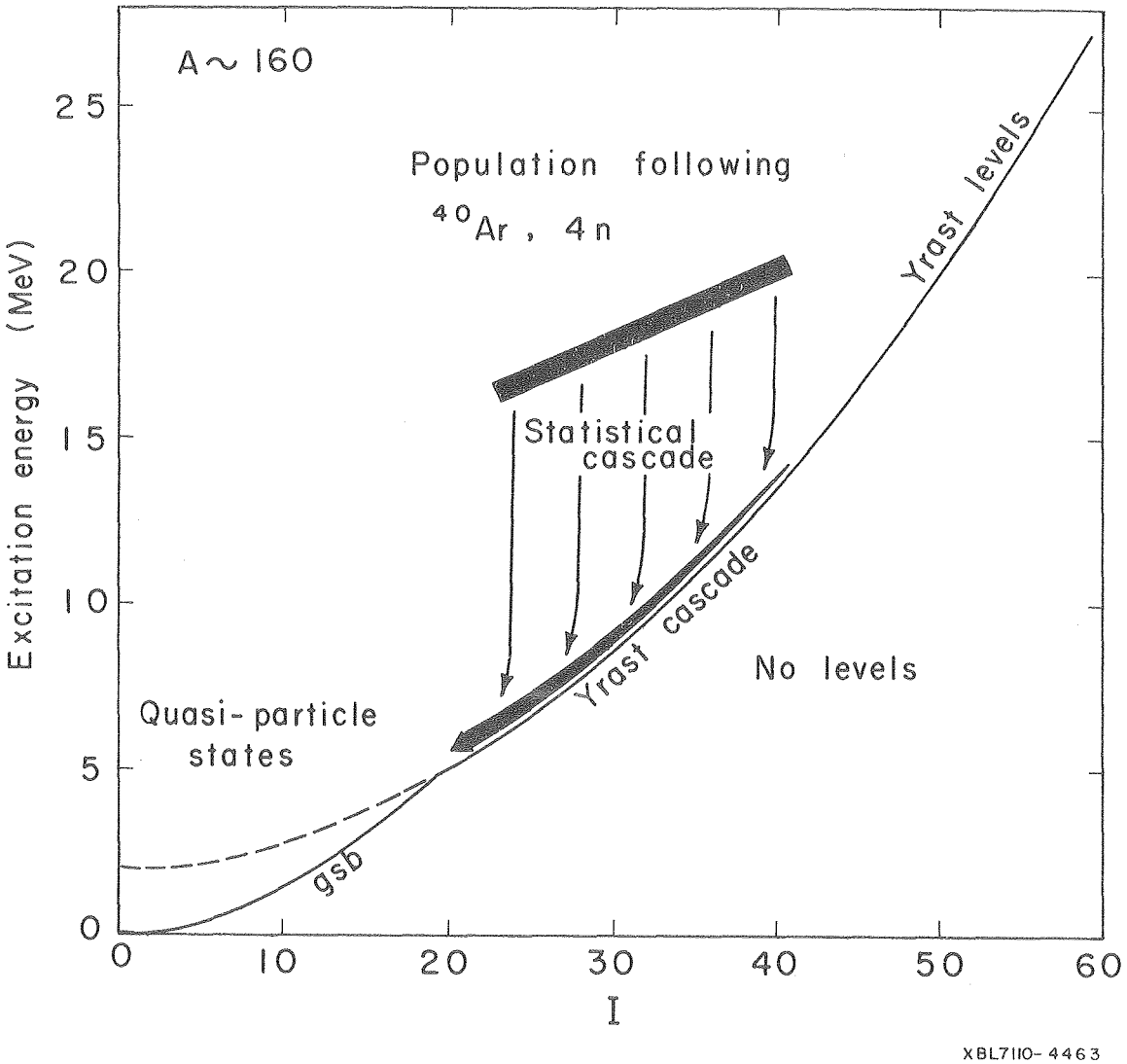

Fig. 4

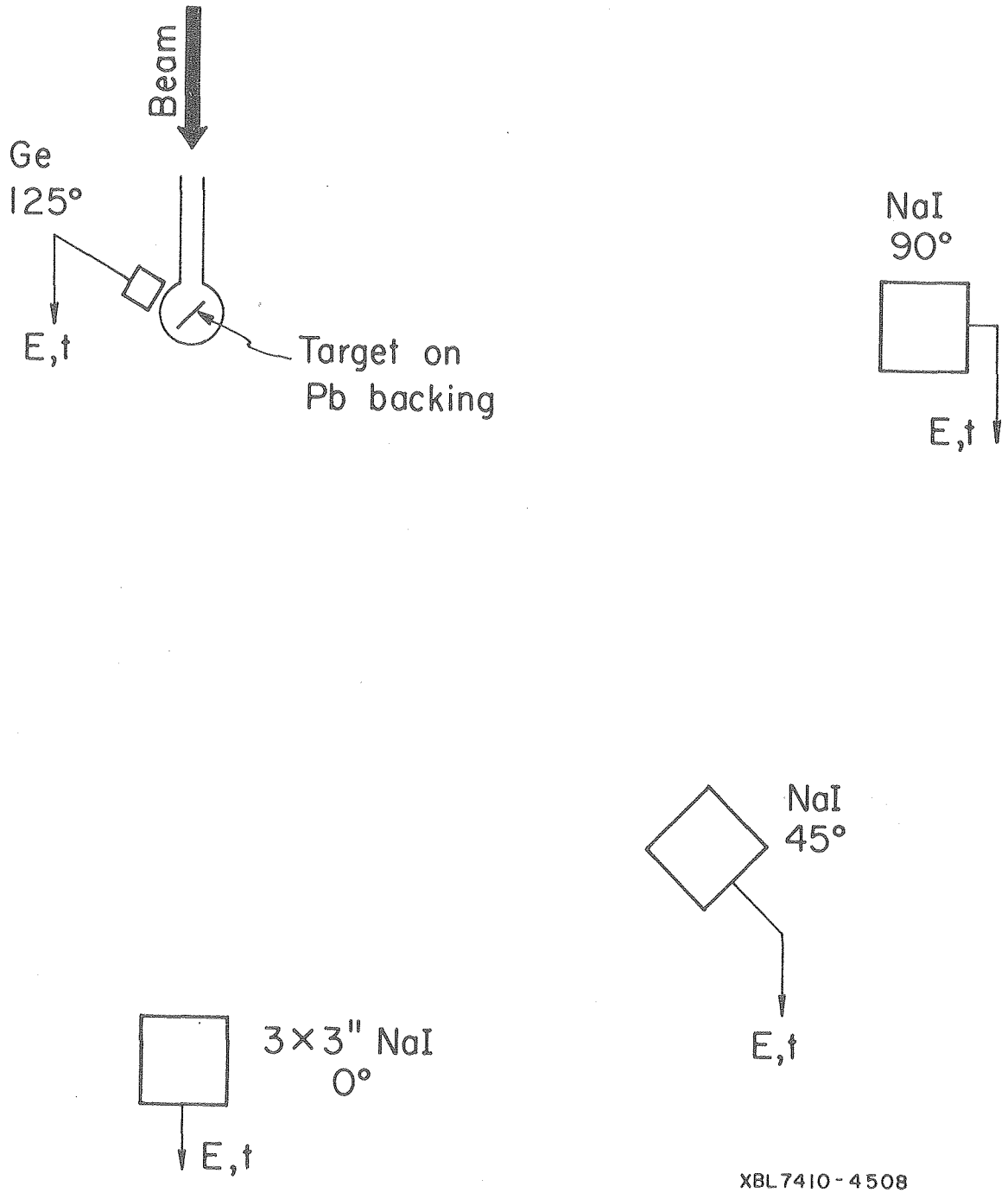
Beam
Ge
125°
E,t
Target on
Pb backing
NaI
90°
E,t
NaI
45°
E,t
3×3" NaI
0°
E,t
XBL7410-4508

Fig. 5

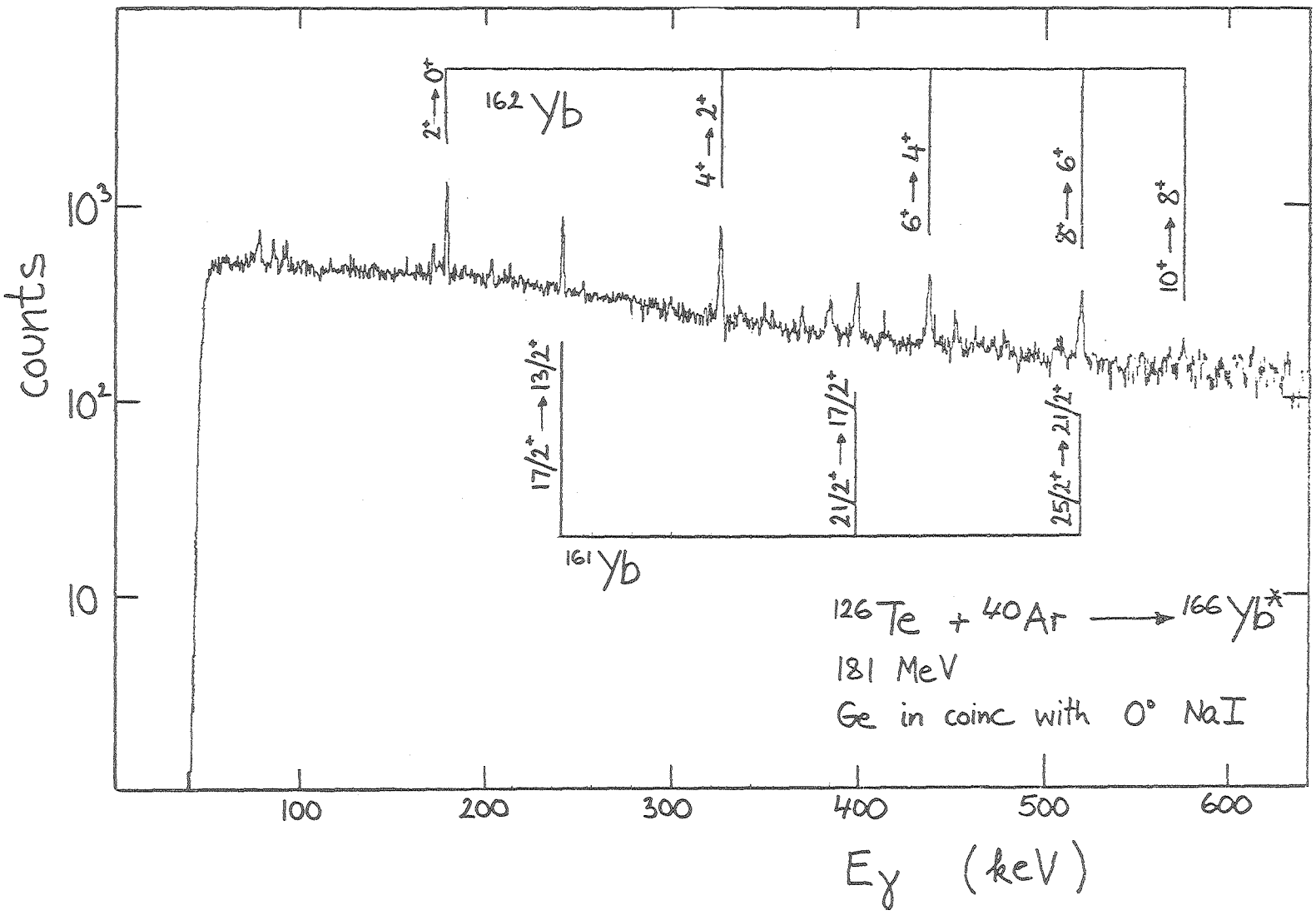

XBL 7512-9841

Fig. 6

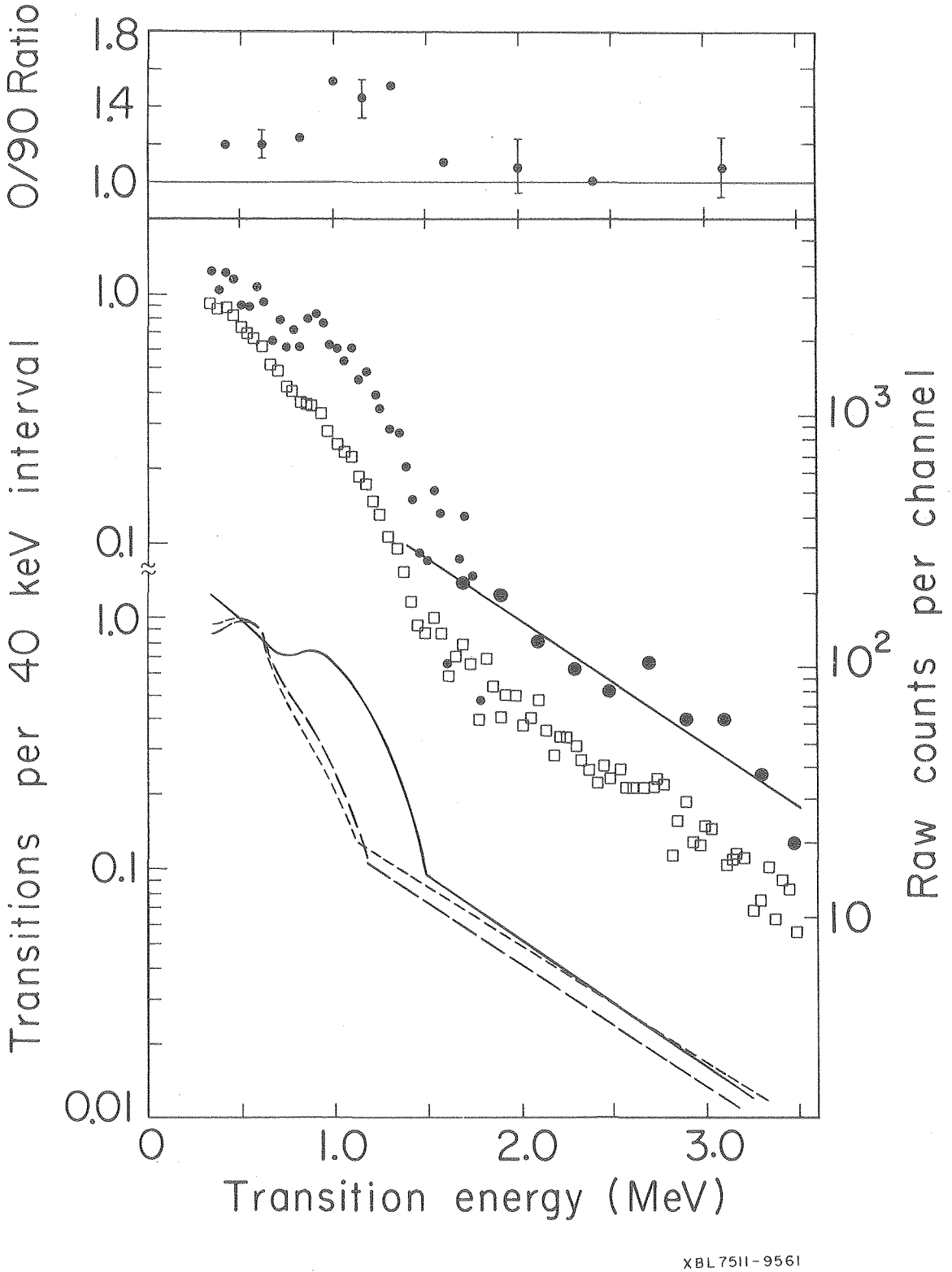
0/90 Ratio
1.8
1.4
1.0
Transitions per 40 keV interval
1.0
0.1
1.0
0.1
0.01
Raw counts per channel
10^3
10^2
10
0
1.0
2.0
3.0
Transition energy (MeV)
XBL7511-9561

Fig. 7

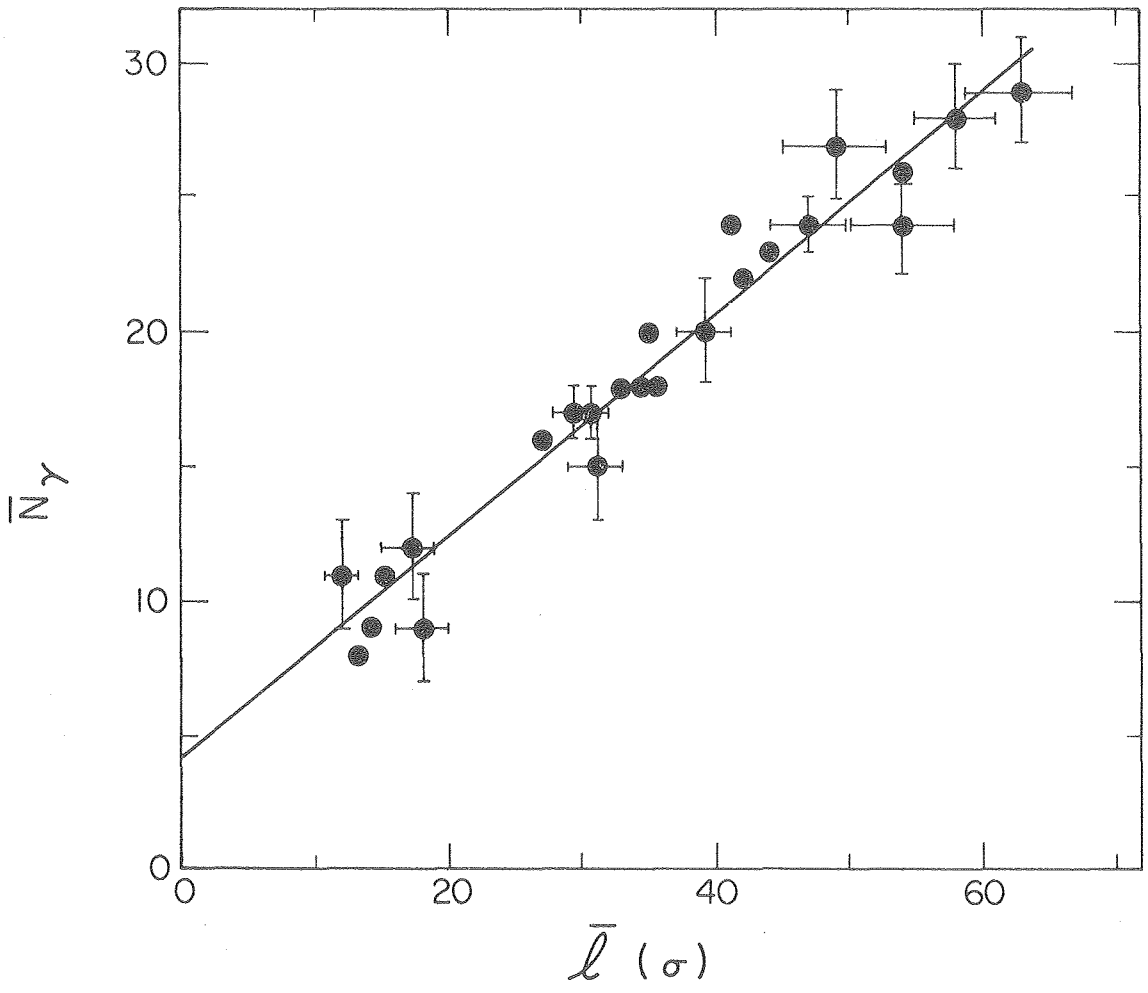

Fig. 8

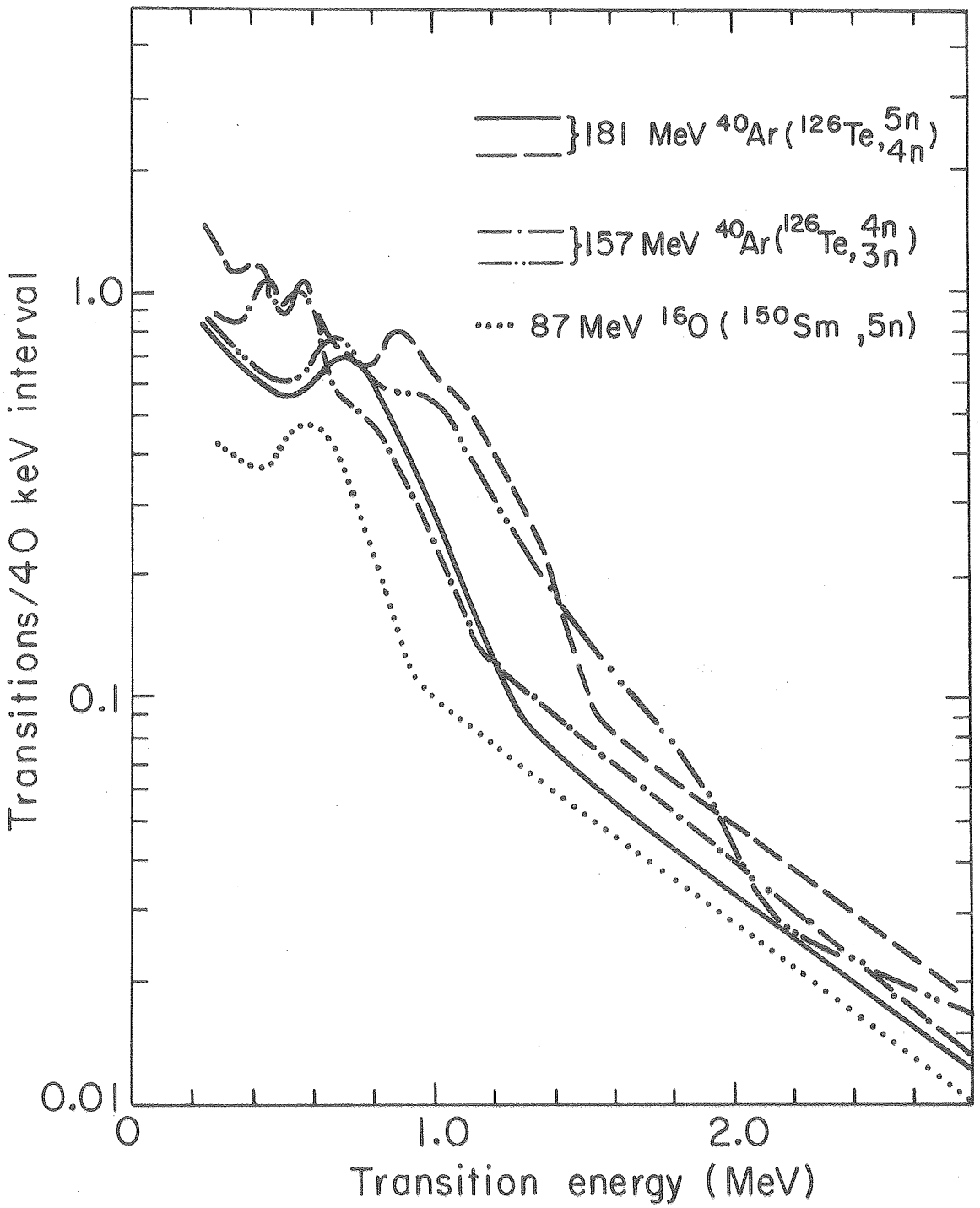

XBL 765-2848A

Fig. 9

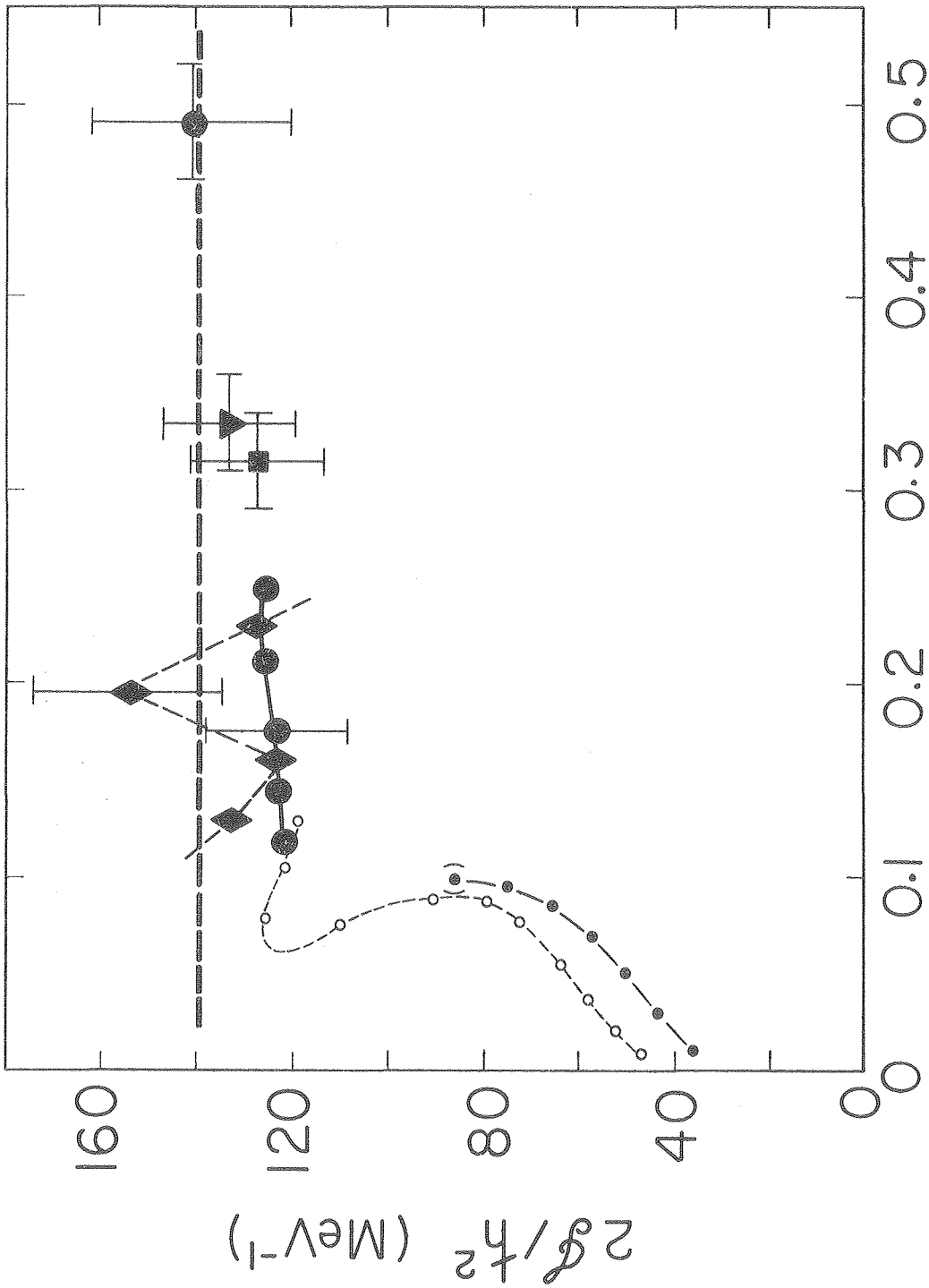

XBL7511-9562

Fig. 10

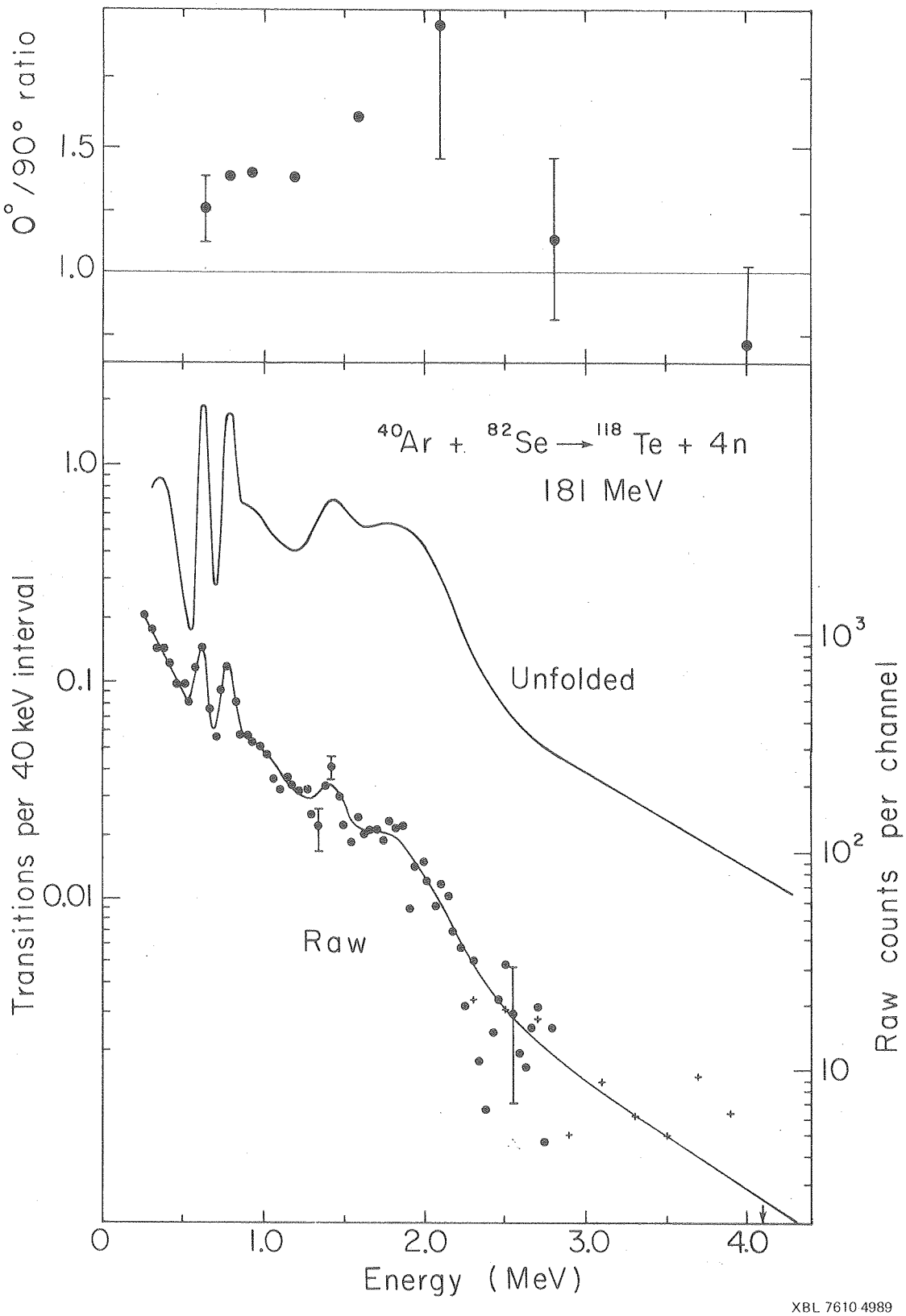
0°/90° ratio
1.5
1.0
$^{40}Ar + {}^{82}Se \rightarrow {}^{118}Te + 4n$
181 MeV
Unfolded
Raw
Transitions per 40 keV interval
1.0
0.1
0.01
10^3
10^2
10
Raw counts per channel
0
1.0
2.0
3.0
4.0
Energy (MeV)
XBL 7610 4989

Fig. 11

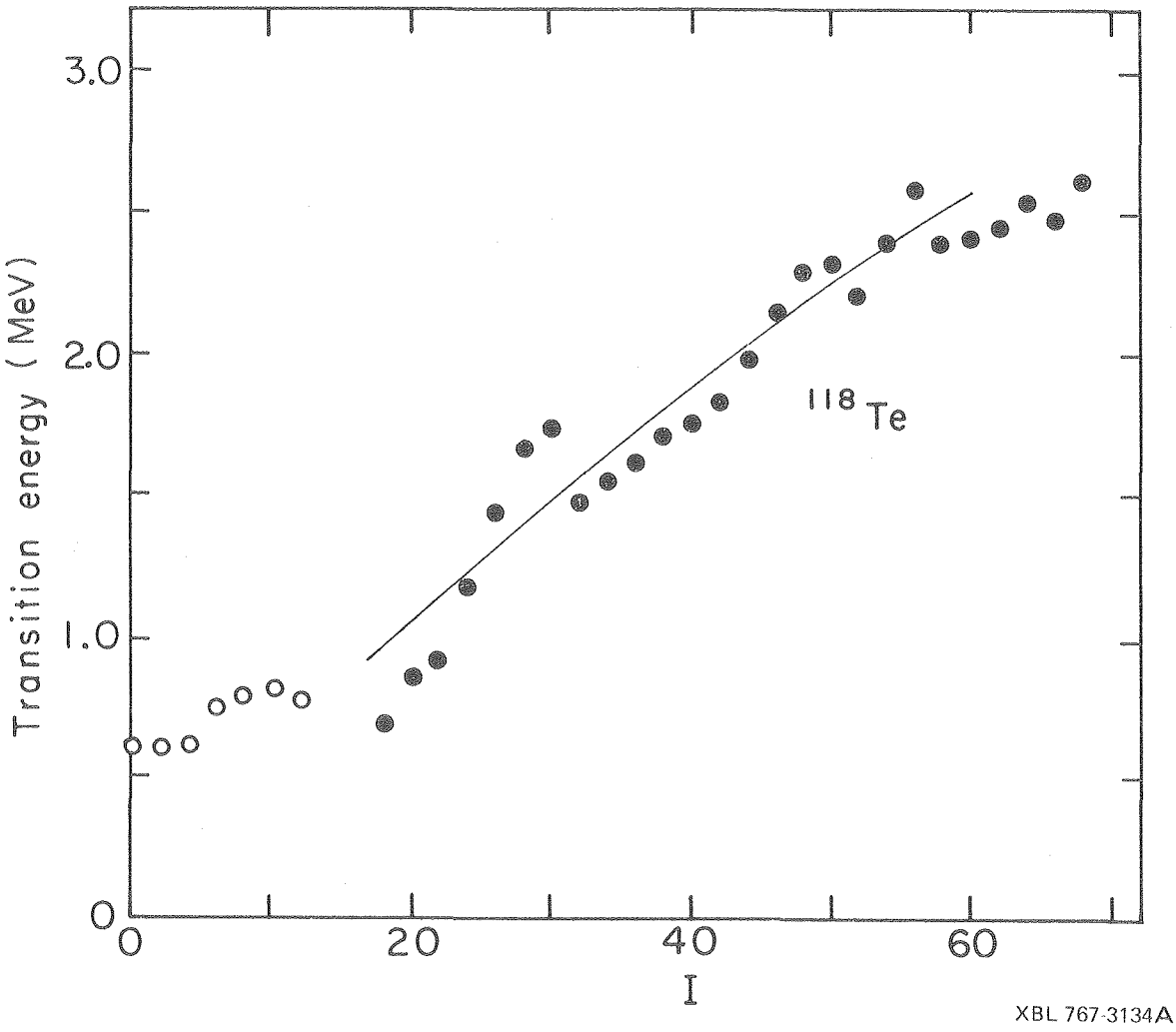

Fig. 12

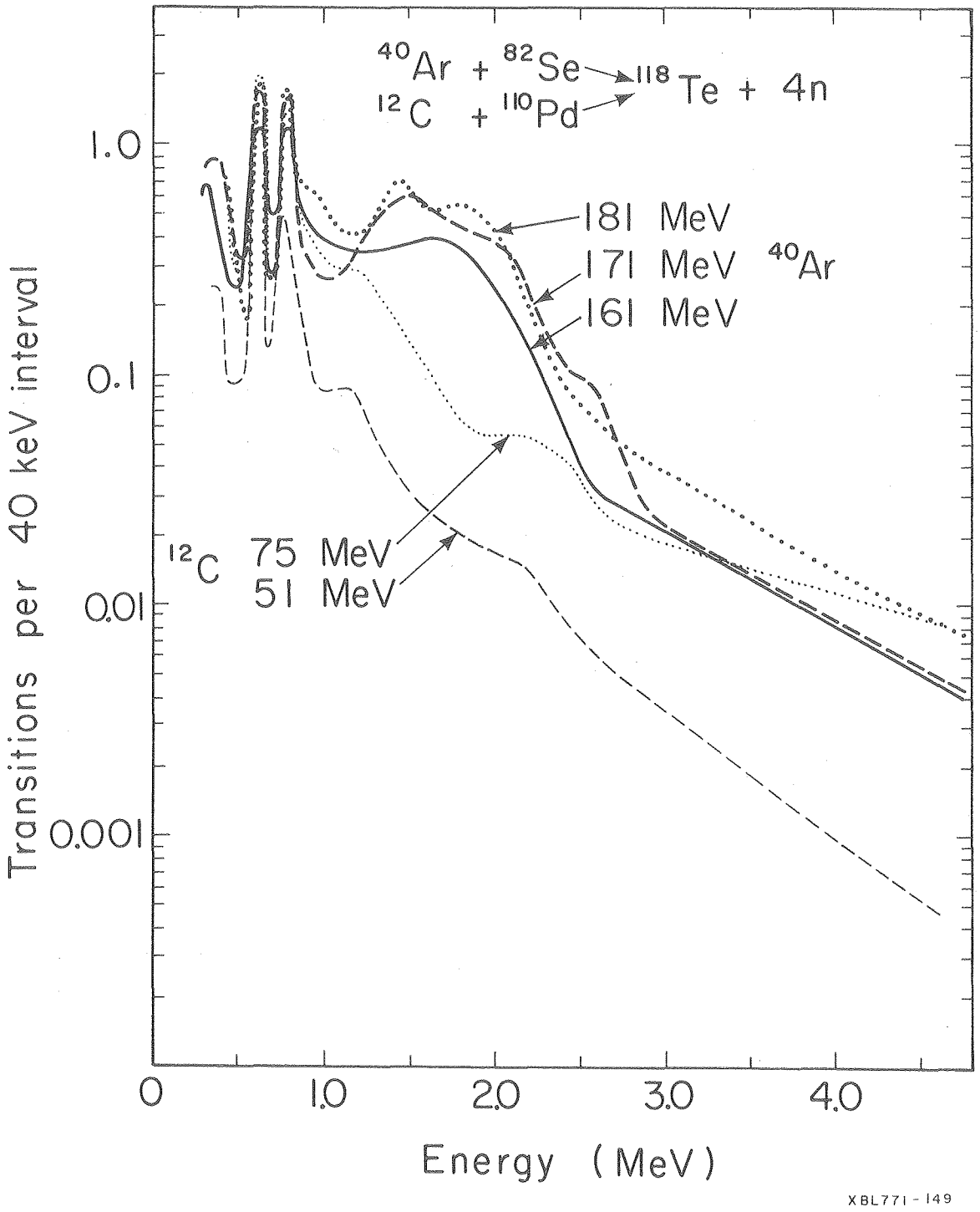
$^{40}Ar + {}^{82}Se \rightarrow {}^{118}Te + 4n$
$^{12}C + {}^{110}Pd$
181 MeV
171 MeV ^{40}Ar
161 MeV
^{12}C 75 MeV
51 MeV
Transitions per 40 keV interval
1.0
0.1
0.01
0.001
0
1.0
2.0
3.0
4.0
Energy (MeV)
XBL771-149

Fig. 13

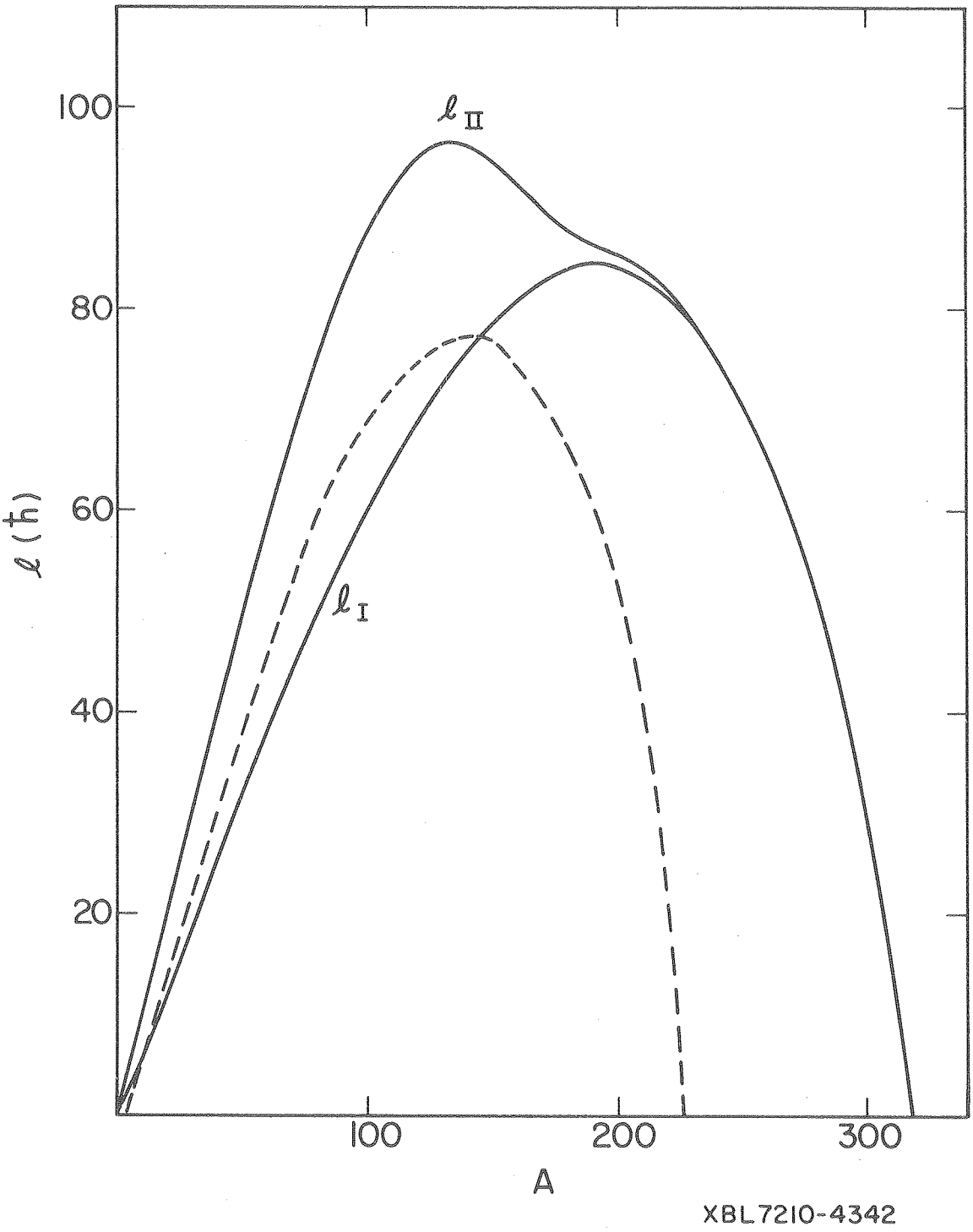

Fig. 14

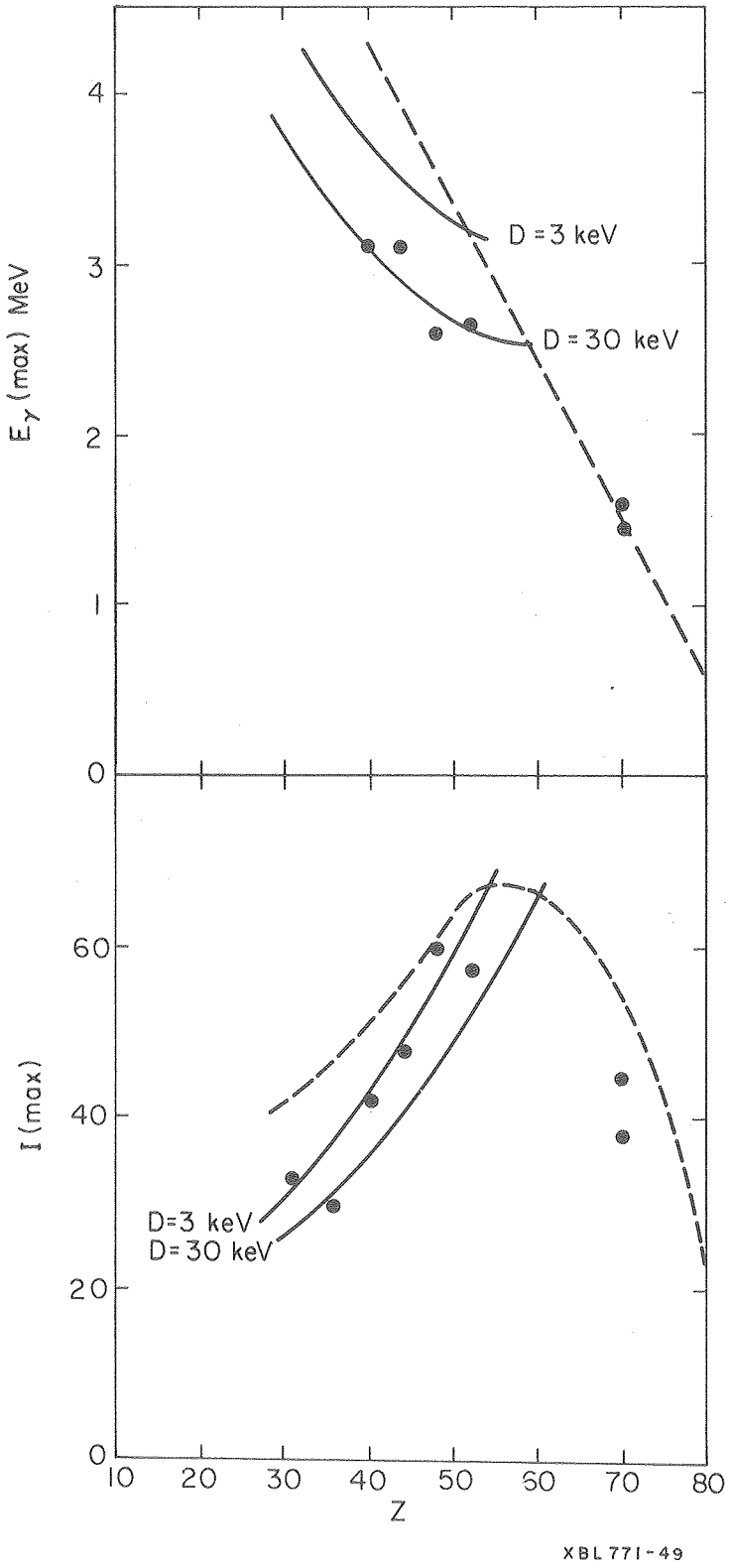
E_γ (max) MeV
4
3
2
1
0
D = 3 keV
D = 30 keV
I (max)
60
40
20
0
D=3 keV
D=30 keV
10
20
30
40
50
60
70
80
Z
XBL 771-49

Fig. 15

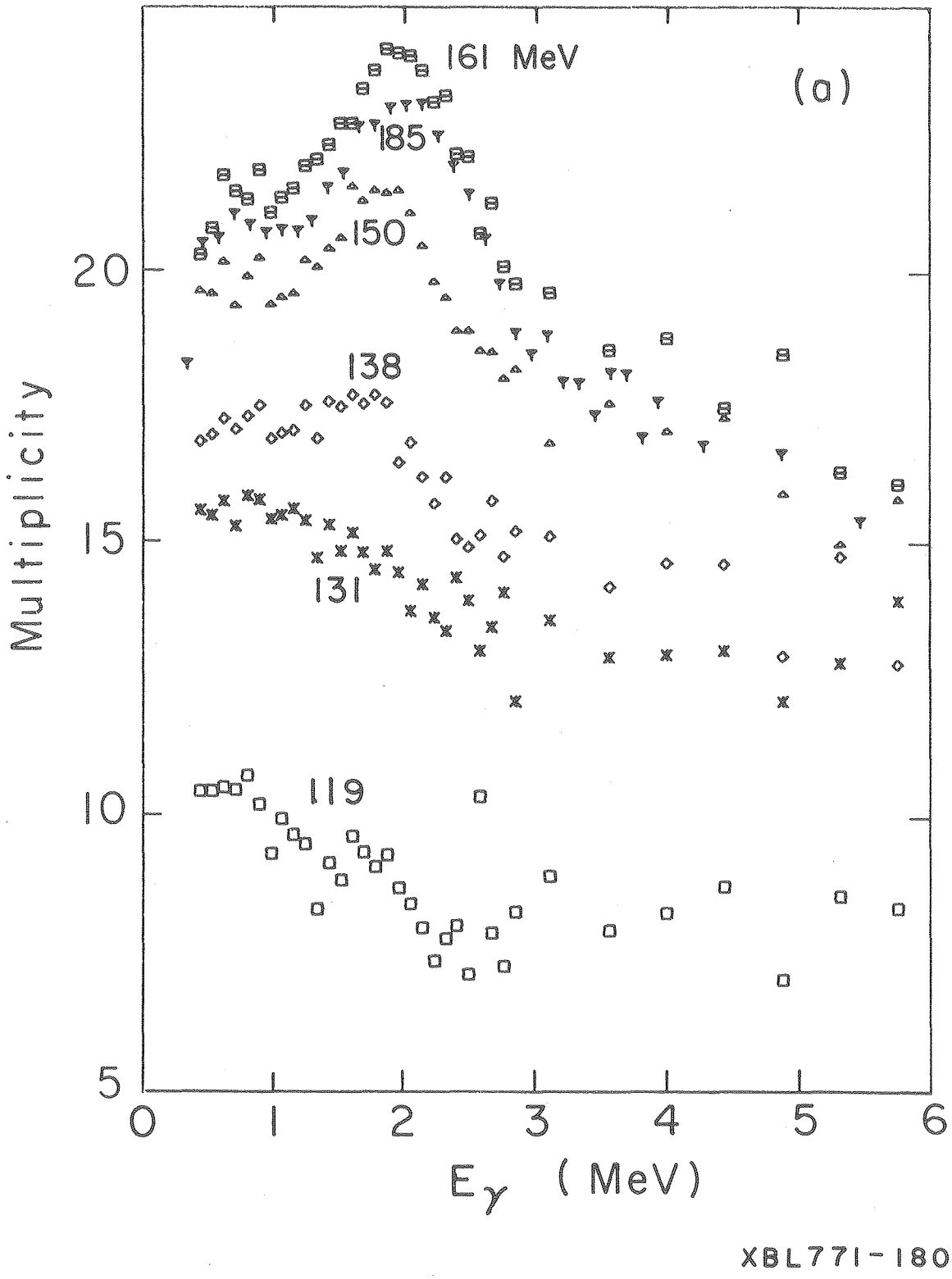

Fig. 16

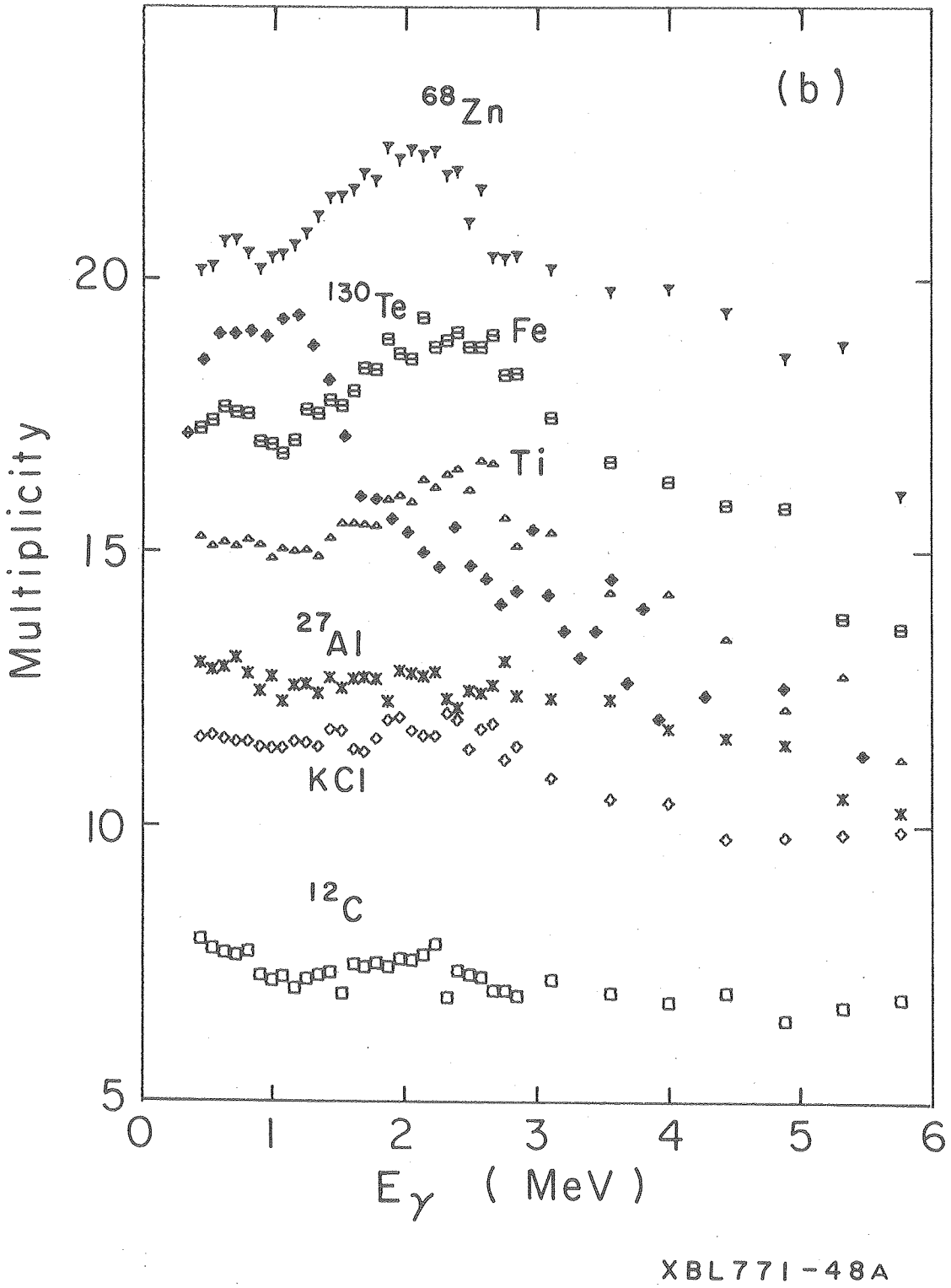
(b)
^{68}Zn
^{130}Te
Fe
Ti
^{27}Al
KCl
^{12}C
Multiplicity
20
15
10
5
0
1
2
3
4
5
6
E_γ (MeV)
XBL771-48A

Fig. 17

This report was done with support from the United States Energy Research and Development Administration. Any conclusions or opinions expressed in this report represent solely those of the author(s) and not necessarily those of The Regents of the University of California, the Lawrence Berkeley Laboratory or the United States Energy Research and Development Administration.